Analysis of extreme rainfall trends based on MEV method with 29 long data series

by

Wenyu Zhou

Student Name	Student Number
Wenyu	5504449

Instructor: Ruud van der Ent
Project Duration: August, 2022 - October, 2022
Faculty: Faculty of Civil Engineering and Geosciences, Delft

TU Delft

Abstract

Since the mid-19th century global temperatures have increased significantly, so does the intensity of extreme rainfall. Previous studies have suggested that by the end of the century extreme rainfall intensity would increase by 10.5% and 28.2% for the low and high emission scenarios, and the centennial extreme rainfall would increase by 13.5% and 38.3%. For this model-based result, our aim is to verify it with observed historical data and find out the growth rate of extreme rainfalls. In this study, the MEV method was used to analyze the changes in the intensity of daily extreme rainfall in the 1-year, 10-year, and 100-year return periods at 29 stations and linearly fit them to determine the trends, and finally found that: the extreme rainfall showed an increasing trend in 70% of the stations in all data years, and the average growth rates in the 1-year, 10-year, and 100-year return period are 9.73%, 8.06% and 12.00%, respectively. From 1950 to the present, 56% of the stations have an increasing trend of extreme rainfall and the growth rate is 6% and 4% for 1-year and 10-year events, 2.4% for the 100-year events. For the growth rate per decade, the 1-year and 10-year events grow faster after 1950 than data from 1850, and the growth rate of the 100-year events becomes smaller.

Contents

1

Introduction

1.1. Background

Climate has warmed significantly since the Industrial Revolution, CO_2 will be the dominant climate change factor in this century. This human-induced climate change has led to an increase in the frequency and intensity of extreme temperature, as well as an increase in extreme precipitation and droughts on a large scale (Allen & Ingram, 2002).

The intensity of extreme rainfall will have a significant impact on society as a result of climate change, and the annual cost to society of extreme rainfall is enormous. Intense rainfall can produce flash floods with very short response times (Elkhrachy, 2015), which is becoming a common natural disaster in many parts of the world. Flooding due to rainfall is one of the most costly and dangerous natural disasters in the world, and has caused 140 million in economic losses in New Zealand over the past decade, and is expected to cause over 52 billion in economic losses worldwide by mid-century (Frame et al., 2020; Hallegatte et al., 2013).

Since 1901, global precipitation has increased at an average rate of 0.04 inches per decade, which is about 1.016mm per decade, and the extreme precipitation events outpacing this trend (EPA, 2021). And the daily extreme rainfall has shown significant increase in both observations and global climate models (Donat et al., 2016).

Most of the precipitation comes from moisture already present in the atmosphere at the start of the storm, so the intensity of the precipitation depends on the available moisture, especially for extreme rainfall events. Thus the simplest prediction of extreme rainfall is that the intensity of rainfall is almost proportional to the moisture at the bottom of the atmosphere, with the water content increasing at a warming rate of Clausius-Clapeyron (CC) value, about 6-7 $\%K^{-1}$ (Trenberth et al., 2003). Other research has shown that extreme rainfall predictions are not applicable in the tropics because the variability of extreme rainfall depends on the variability of the decreasing rate of wet adiabatic temperature, the rate of rise, and the temperature at which extreme precipitation occurs (O'Gorman & Schneider, 2009).

Changes in extreme rainfall may show opposite trends in space, with greater heterogeneity compared to increasing temperature warming (Donat et al., 2013). Baseing on a coupled model organized by the Fourth Assessment Report (AR4), some researches concluded that arid regions become drier while wet regions become wetter because the magnitude of atmospheric moisture convergence and divergence is expected to increase with increasing atmo-

spheric moisture content (Held & Soden, 2006). Despite the different trends of increasing or decreasing extreme rainfall in different wet and dry regions, an increasing trend was observed in most of the regions (Donat et al., 2016).

1.2. Previous researches

The trend of rainfall variation is an important phenomenon to be considered, and analyzing the variation of rainfall in historical data is a great reference value for studying and predicting the trend of rainfall changes in the future.

Many studies focused on rainfall variability. The analysis of common rainfall trends was mainly performed using the Mann-Kendall method. Such as Cislaghi et al. used rainfall data from four stations in Italy to analyze historical changes in annual rainfall, rainfall intensity, and rainfall events. A negative trend in annual precipitation was found in the first half of the 20th century, followed by a positive trend in northern Italy (Genoa, Milan and Bologna). In contrast, the dataset from Palermo (southern Italy) shows only negative trends. The analysis of monthly rainfall trends in Turkey by Partal and Kahya, revealed that a significant decrease in mean annual precipitation was observed in western and southern Turkey and in the Black Sea coastal region. Zhai et al. analyzed rainfall data from 740 stations in China and concluded that there was little overall precipitation variation during 1950-2001, but there were clear regional and seasonal trends.

For extreme rainfall, Y. Wang and Zhou concluded that summer extreme precipitation events in the Yangtze River basin increased sharply by 10%-20% per decade from 1961-2001, consistent with the trend of increasing average summer precipitation in the region. Kunkel et al. analyzed trends in short-term (1-7 day) extreme precipitation events with repeated intervals of 1 year or longer for U.S. and Canadian stations and found that the national trend for the U.S. was to increase at a rate of 3% over the decade. The trend for the United States was found to rise at a rate of 3% over the decade, during the period 1931-96. Although the annual trend for Canada was upward during 1951-93, it was statistically insignificant. For extreme rainfall in Europe, Zolina et al. clearly reveal an increased incidence of extreme precipitation in western European Russia (up to 4% /decade), with a decreasing trend in the partial contribution of very wet weather found in Central Western Europe during the summer months.

Many studies have been conducted on extreme rainfall using Gumble, Peak Over Threshold (POT), Generalized extreme value (GEV) and Metastatistical Extreme Value framework (MEV) (H. Wang & Xuan, 2022; Das et al., 2022; Yue et al., 2022; Fofana et al., 2022).

For example, Fofana et al. used the Gumbel extreme value distribution to analyze extreme rainfall and flood recurrence periods in the city of Bamako, Mali, in West Africa and found an increase in the intensity and frequency of extreme rainfall. POT method was applied by McBride et al. to analyze data from 70 stations in South Africa from 1921-2022 and concluded that there is a general increase in the likelihood of experiencing significant and extreme daily rainfall events over most of South Africa. Amponsah et al. used the Simplified MEV to model extreme rainfall quantiles in tropical regions and found an increase in extreme daily rainfall over the period 1978-2018 in Volta basin.

Compared to the systematic errors of the GEV and Gumble methods, there is excellent coherence between the MEV estimates and the 'observed' frequency of extreme events in the generated synthetic time series (Marani & Ignaccolo, 2015). The MEV method has a great advantage in analyzing long return periods of extreme rainfall in short-term records. With a

sufficient number of rainfall events per year, the MEV method can even generate information on the 100-year return period quantile of the 5-year rainfall data (Marra et al., 2018). The MEV distribution also shows a large improvement in accuracy compared to previous methods, Miniussi and Marani found that to improve the accuracy of short-term observations, the MEV distribution can better resolve fluctuations in the high quantile and allow for long-term trends above the estimated noise. Hosseini et al. applied the MEV distribution to the analysis of extreme Atlantic hurricanes, improving the accuracy of its estimates by 50%.

In summary, the MEV distribution has excellent ability to calculate extreme rainfall in short-term data (even in 5 years), as well as high accuracy with small error, and therefore was applied to this study to calculate extreme precipitations.

1.3. Goal of this work: Analysis of extreme rainfall trends over 100 years

Anthropogenic greenhouse gas increases lead to an intensification of the observed heavy precipitation events, which are found in about two-thirds of the data coverage of the Northern Hemisphere land area (Min et al., 2011).

In order to predict the effect of CO_2 emissions on temperature as well as rainfall under different emission scenarios, CMIP Phase 6 (CMIP6) was applied for future climate prediction (L. Wang et al., 2022). Gründemann et al. analyzed that the annual rainfall extremes would increase by 10.5% and 28.2% for the low and high emission scenarios by the end of the century, and the centennial extreme rainfall would increased by 13.5% and 38.3%, respectively. However, this result is only predicted by the model and not verified by historical data.

To demonstrate this increasing trend of extreme rainfall, the stations with more than 100 years of recorded data will be selected for this study to analyze the trend of extreme rainfall with available data. If we get a trend of extreme rainfall increase in the historical data, we can assume that there will be such an increase at the end of this century as well. In addition, CO_2 emissions have increased a lot since we entered the modern era, and we are curious about how this scenario will affect extreme rainfall. Therefore, data after 1950 were also chosen for the trend analysis.

2

Methods

2.1. Metastatistical extreme value (MEV)

The MEV method was firstly proposed by Marani and Ignaccolo, which is defined in terms of the distribution of the statistical parameters describing “ordinary” daily rainfall occurrence and intensity. Using the MEV method, the restrictive assumptions of the classical EVT are relaxed, by treating the parameters that defining the number of events and the probability distribution of event sizes as random variables.

Zorzetto et al. has given a more detailed explanation in their study. The MEV method considers the number of events n, parameters $\vec{\theta}$, of the parent distribution in each block, as random variables (N and $\vec{\Theta}$). The randomness of the parameters of the number of events and the magnitude of the events explains two things:

1) the stochastic process of rainfall event occurrence, i.e., the generation of a finite and variable number of rainfall events within the scale of each year.

2) The frequency distribution of possible changes in the magnitudes of rainfall events in different years.

If the total probability theory is used and all possible distributions of the number of events N and parameters $\vec{\Theta}$ are considered, the cumulative distribution function of the MEV would be as shown in Eq.2.1.

$$\zeta(x) = \sum_{n=1}^{\infty} \int_{\Omega_{\vec{\theta}}} F(x;\vec{\theta})^n g(n,\vec{\theta}) \mathrm{d}\vec{\theta} \tag{2.1}$$

where $g(n,\vec{\theta})$ is the joint probability distribution of N and $\vec{\Theta}$, and $\Omega_{\vec{\theta}}$ is the population of all possible values of the parameters.

Daily non-zero rainfall has been shown to be accurately modeled as a Weibull variable, can be written as

$$F(x;C,w) = 1 - e^{-\left(\frac{x}{c}\right)^w} \tag{2.2}$$

where C and w being, respectively, the Weibull scale and shape parameters.

And thus define the MEV-Weibull cumulative distribution function as

$$\zeta(x) = \sum_{n=1}^{\infty} \int_C \int_w g(n, C, w) \cdot \left[1 - e^{-\left(\frac{x}{C}\right)^w}\right]^n \, \mathrm{d}C \, \mathrm{d}w \tag{2.3}$$

where the second part, $F(x; C_j, w_j)$, is the Weibull distribution, and $j(j = 1, 2, ..., M)$, is the observations of each years.

So that the annual maximum daily rainfall depth, i.e., the maximum depth for n wet days in a typical year, is distributed as

$$H_{n_j}(x) = F\left(x; C_j, w_j\right)^{n_j} \tag{2.4}$$

where n_j is the wet days in year j.

And the mathematical expectation in Eq.2.1 is replaced by the approximate mean value, and the expression is

$$\zeta(x) \cong \zeta_m(x) = \frac{1}{M} \sum_j F\left(x; C_j, w_j\right)^{n_j} \tag{2.5}$$

Thus, the discrete expression for MEV is as

$$\zeta_m(x) = \frac{1}{M} \sum_{j=1}^{M} \left[1 - e^{-\left(\frac{x}{c_j}\right)^{w_j}}\right]^{n_j} \tag{2.6}$$

The probability weighted moments method (PWM) was used to fit the Weibull distribution to the observed values for each year to give greater weight to the tails of the distribution, in order to obtain better simulated values of extreme rainfall.

2.2. Dataset

Stations with more than 100 years of daily rainfall data will be selected for this study. Many of the recordings can be found in NOAA's Global Historical Climatology Network (GHCN), while others are from private contacts. Among them, 19 sites have data based on Zorzetto's original data extended to the most recent GHCN data record, and 10 directly use the original private contact data (Zorzetto et al., 2016).

The stations and starting and ending years of the data are shown in the table in the Appendix A.1, with an average record length of 174 years. The longest recorded site is Padova, with 288 years of recorded data. Most of the sites are from Europe, with a small number from the North America and Australia.

The location of the stations is as figure 2.1.

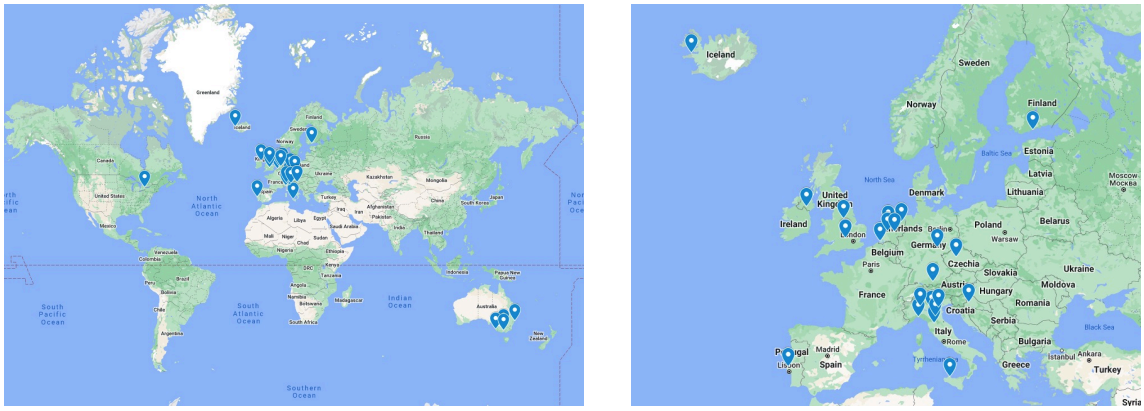

Figure 2.1: Location of the stations

2.3. Data Processing

2.3.1. Creation of the moving window

This study uses the MEV framework to determine the intensity of extreme rainfall in the data. Because of the good performance of the MEV method in calculating extreme rainfall in short-term data for high return periods, a 30-year block was selected to calculate extreme rainfall for the available data.

To obtain the trend of extreme rainfall variability, a moving window was made to take 29 years backward for each year of data (for a total data length of 30 years), and the mevpy package was called for the window. For example, if the years of data recording are from 1897-2017, then the window takes 1897-1926, 1898-1927, 1899-1928, ... , 1988-2017.

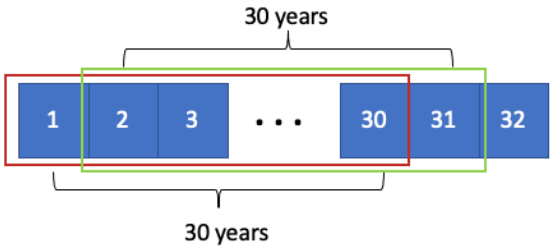

Figure 2.2: The 30-years slider of each year

The continuity of extreme rainfall for each window that calculated in this way is stronge (because only one year of data is changed) and it is easier to see the trends of the extreme rainfall variation.

2.3.2. Inspection of the parameters

In the use of the MEV package, the determination of some parameters is crucial. For example, n, the dimension of the sample (also known as wet days in a year), should exceed $1mm/day$. The Weibull parameter C, w also needs to be greater than 0. Therefore, when calling the mevpy function, the number of wet days in a year and the weibull parameter should be checked first.

Since there are many overlaps in the calculation of extreme rainfall and the parameters n, C , w need to be used repeatedly, and these three parameters take a long time to calculate, the

parameters need to be calculated and checked in advance before calling the function.

Another key input value is x_0. The parameter x_0 is the starting guess for the numerical solution of the MEV and is an initial guess that needs to be inputted to call the function. However, rainfall varies greatly from region to region, and x_0 that applies to one region may not apply to another, and the program may not find a suitable numerical solution.

In this case, we need to guess different values of x_0 and change x_0 in case of warnings. If none of these guesses satisfy the conditions for an available solution, the calculated result needs to be replaced by -999.

2.4. Data analysis

In this study, rainfall for the 1-year-return period, 10-year-return period, and 100-year-return period were chosen as the non-exceedance probability, F. Finally we will obtain continuous data of these three rainfall periods at each station.

A linear regression with least-squares method is applied to the trend analysis. We are able to obtain the slope of the linear fit and thus the rate of change of the extreme rainfall over the calculated time period, the equation is as

$$y = \beta_0 + \beta_1 x \tag{2.7}$$

If it shows a positive slope, $\beta_1 > 0$, in a unit of $mm/year$, then it indicates an increasing trend of rainfall intensity each year during the analyzed time. The opposite is an indicative of decrease.

And the growth rate G_R (%) can be written as

$$G_R = \frac{P_1 - P_0}{P_0} \tag{2.8}$$

Where P_0 and P_1 represent the extreme rainfall intensity of the earliest years and latest years, mm/day.

Calculating the growth rate for each decade allows us to determine the magnitude of the growth rate for different periods.

$$G_{\text{decade}} = \frac{G_R \times 10}{n} \tag{2.9}$$

Where G_{decade} is the growth rate in a decade, $\%/decade$, n is the years length.

2.5. Significance test

2.5.1. Student's t-test

The t-test is used to determine whether the means of two samples are significantly the same, and can also be used for one sample and a specified mean value.

In the one sample t-test, the stastic is like:

$$t = \frac{Z}{s} = \frac{\bar{X} - \mu}{\widehat{\sigma}/\sqrt{n}} \tag{2.10}$$

Where $\bar{X}$ is the he sample mean, $\widehat{\sigma}$ is the estimate of the standard deviation of the population, and μ is the population mean.

The α is set to 0.05, also using a one-tailed distribution, which means that there is a 5% risk of concluding that there is a difference between them when the unknown overall mean is the same.

2.5.2. Spearman's rank correlation coefficient

The Spearman rank correlation coeffcient is a nonparametric technique for evaluating the degree of linear association or correlation between two independent variables (Gauthier, 2001). It is a parentless indicator that measures the correlation of two variables. It uses a monotonic function to evaluate the correlation of two statistical variables. The Spearman correlation coefficient is +1 or -1 if there are no repeated values in the data and when the two variables are perfectly monotonically correlated (Wikipedia, 2022).

The Spearman correlation coefficient is defined as the Pearson correlation coefficient between the rank variables (Myers & Well, 2003).

$$r_s = \rho_{R(X),R(Y)} = \frac{cov(R(X), R(Y))}{\sigma_{R(X)}\sigma_{R(Y)}} \tag{2.11}$$

Where ρ denotes the usual Pearson correlation coefficient, but applied to the rank variables,

$cov(R(X), R(Y))$ is the covariance of the rank variables,

$\sigma_{R(X)}$ and $\sigma_{R(Y)}$ are the standard deviations of the rank variables.

3

Results analysis

3.1. Extreme rainfall tendency of recording years (since 1850)

Here we plotted the 30-year extreme rainfall values calculated from all available data for all stations. After fitting it with linear regression to obtain the slope of the optimal fitted line, as table 3.1. The order of the stations was sorted by rainfall intensity from smallest to largest, it can be found that the slopes fitted to the data for most of the stations are positive.

Table 3.1: Slopes of linear regression fit for available data, mm/year

Station	**slopes (**mm/year**)**		
	1-year return period	10-year return period	100-year return period
Putten	0.002	0.003	0.002
Oxford	0.000	0.000	0.004
Hoofdoorp	0.003	0.004	0.007
Sheffield	0.004	0.002	0.017
Melbourne	0.000	0.003	0.004
Zagreb	0.000	0.001	0.010
Bologna	0.000	-0.005	-0.008
Padova	0.001	0.003	0.008
Milano	0.004	0.012	0.027
Genova	0.006	0.026	0.048
Stykkisholmur Is	0.046	0.074	0.124
Jena Sternwarte Gm	0.011	0.009	-0.008
Vlissingen Nl	0.044	0.024	-0.020
Prague	0.005	0.019	0.046
Armagh	-0.011	-0.031	-0.061
Eelde	0.022	0.036	0.048
Den Helder	0.023	0.035	0.057
Helsinki	0.007	0.015	0.039
Radcliffe	-0.008	-0.012	-0.019
Robe Comparison As	0.015	0.012	0.009
Deniliquin Wilkinson St As	-0.036	-0.066	-0.203
Palermo It	-0.027	-0.071	-0.116
Mantova It	0.026	0.013	0.004
Hohenpeissenberg Gm	0.057	0.068	0.082
Toronto Ca	-0.007	-0.035	-0.091
Lisbon	0.055	0.115	0.145
Florence	0.003	0.016	0.044
Newcastle Nobbys Signal Statio As	-0.063	-0.214	-0.452

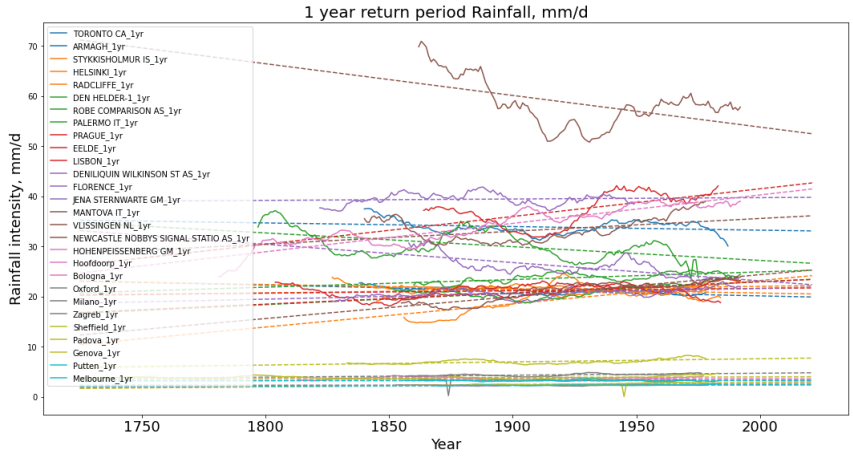

(a)

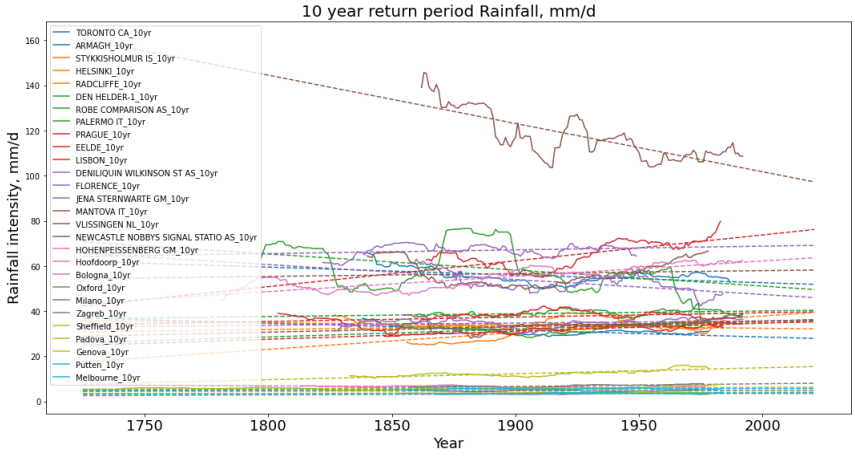

(b)

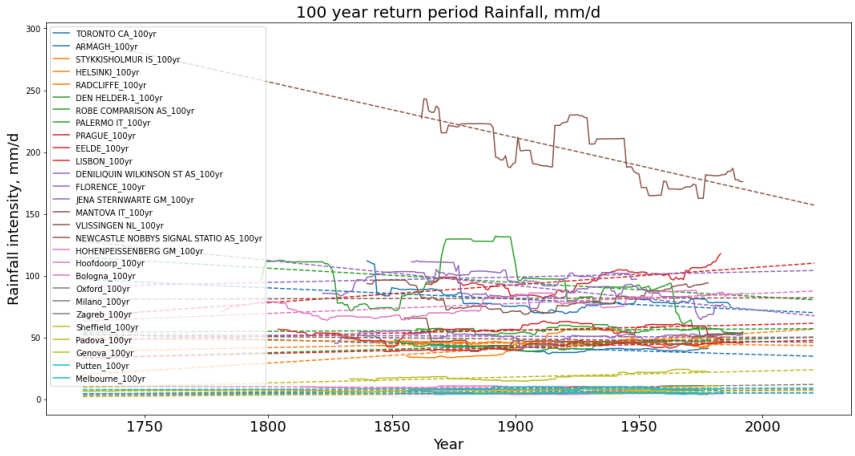

(c)

Figure 3.1: The extreme rainfall tendency in all available data, with a. The 1-year-return period, b. The 10-year-return period and c. The 100-year-return period.

This linear fit can only give a trend simulation, not an accurate numerical increasing. In the figure 3.1, the extreme rainfall data of the stations were very volatile, and some of them even showed a clear cyclical trend. But overall, most of the fitted lines showed an increasing trend, which indicated an increase in the intensity of extreme rainfall over the past 172 years.

One notable exception was NewCastle in east Australia at the top of the figure, which had the strongest extreme rainfall intensity of all stations, but also showed the strongest decreasing trend during the recording years.

In the figure 3.2, we give the growth rates of extreme rainfall for all stations over the data years, from 1850-2022. Although the growth was not large in terms of the slope of the fitted line, an increase could be seen when the percentage of growth rate was calculated. For nearly 70% of the stations, the extreme rainfall showed an increasing trend. The growth rates of extreme rainfall in some areas were very large, such as Stykkisholmur in Iceland, where extreme rainfall in the 1-year, 10-year, and 100-year return periods have increased by more than 100%. For Newcastle and Deniliquin in Australia, both regions showed a trend of decreasing extreme rainfall for the three return-periods, in addition to Palermo in Italy and Toronto in Canada. There were also some regions where the three growth rates varied a lot, such as Milan, Padova in Italy, Zagreb in Croatia, and Vlissingen in the Netherlands, which their growth rates of 100-year return period extreme rainfall could be 5 times larger than that in 1-year return period.

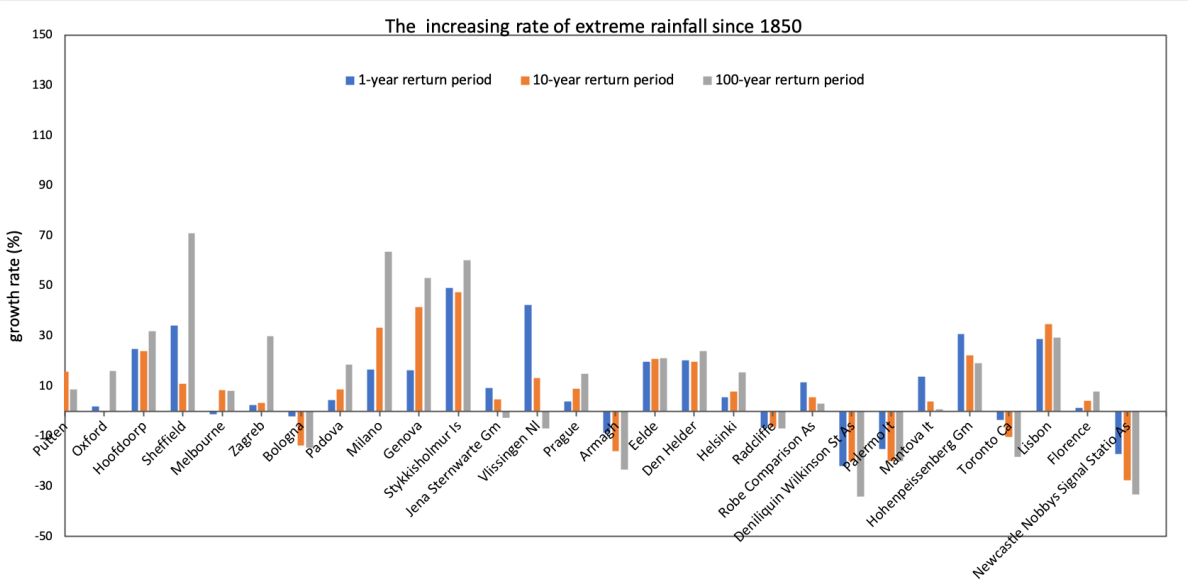

Figure 3.2: The increasing rate of extreme rainfall in all stations, [%]

As shown in the figure 3.3, for the extreme rainfall in the left, 1-year-return period extreme rainfall, the growth rate was most concentrated between 0 and 0.1 for 1-year extreme rain, 10-year and 100-year extreme rainfall. More values fall in the range greater than 0, which showed a generally increase trend. 10-year and 100-year return period rainfall had a similar trend, but was less concentrated than 1-year, and a higher range of distribution could be seen on the left and right side of 0. As the box plot figure 3.3, the 10-year had a longer box section and indicating that it had more variability. However, more growth data overall. For the 100-year extreme rainfall growth rate, it had the greatest variation, with the largest range of boxes in the box plots and a more distant extreme value distribution. From the histogram in figure 3.3,

most of the data fall in the -0.5 to 1 range (50% decrease to 100% increase).

Overall, the distribution of all three rainfall growth rates showed a tendency to be greater than 0. The extreme rainfall in the 100-year return period had a maximum growth rate and a maximum variance, while the rainfall in the 1-year and 10-year return periods was relatively stable and certain.

Table 3.2: The percentage of stations showing an increasing trend and the average growth rate in all recording years

	1-year rerturn period	10-year rerturn period	100-year rerturn period
The percentage of stations with an increase [%]	71.43	71.43	67.86
Average growth rate in all station since 1850[%]	9.73	8.06	12.00
Average growth rate per decade since 1850[%/decade]	0.56	0.47	0.70

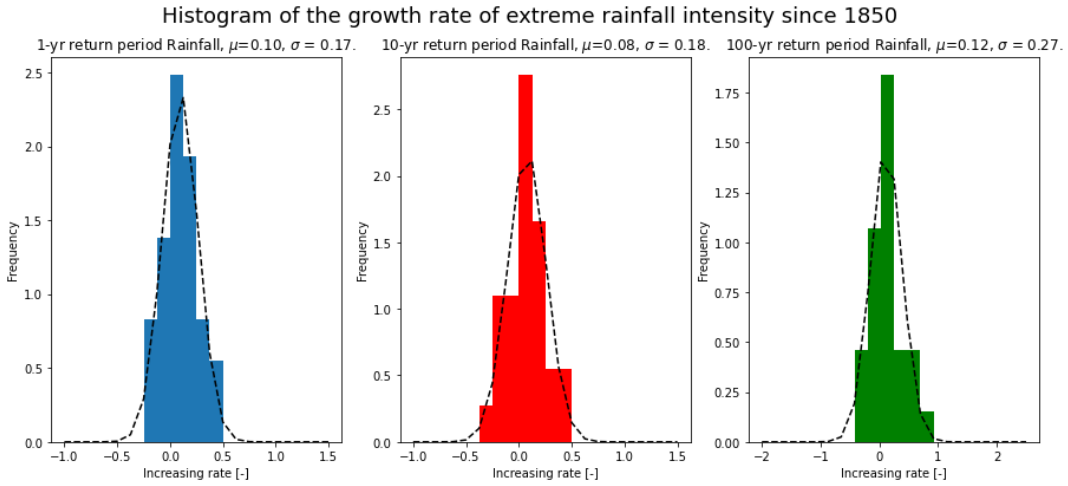

(a)

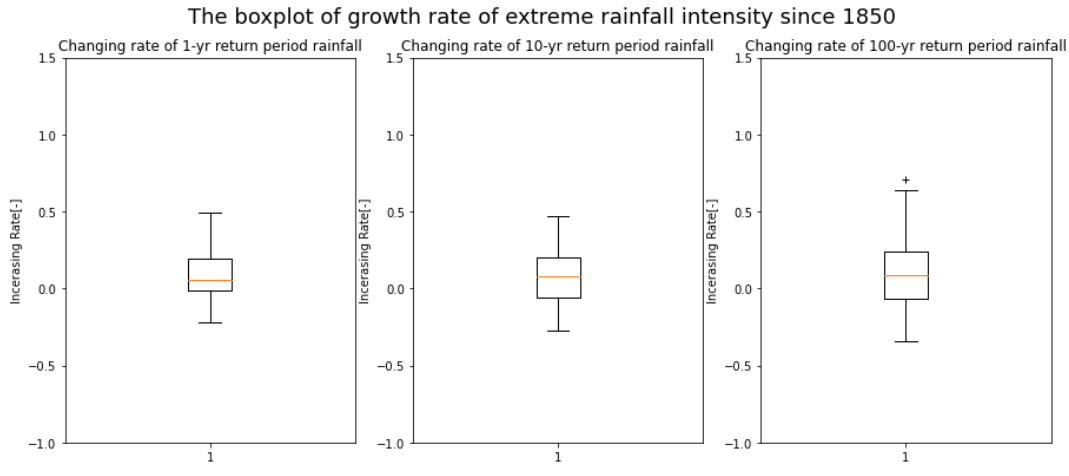

(b)

Figure 3.3: a.Histogram and b.boxplot of growth rate in all stations for left.1-year-return period, middle.10-year-return period, right.100-year-rerturn period

From the table 3.2, the rainfall intensity of the 1-year-return period increased by 9.73%

Table 3.3: T-stastic test values and p-value of three extreme rainfall growth rate of data from 1850

	1-year return period	10-year return period	100-year return period
t-statistic	15.61	12.09	12.12
p-value	2.43E-15	1.05E-12	9.81E-13

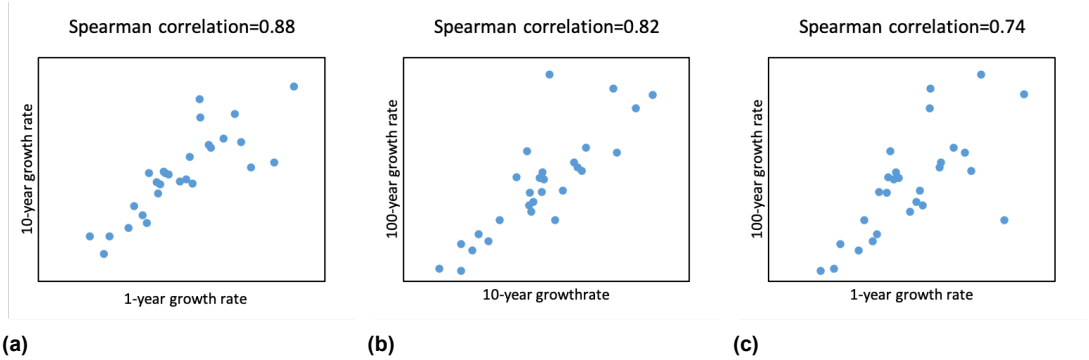

Figure 3.4: Spearman rank test of growthrate between three extreme rainfall since 1850, for 1-year and 10-year events in a, 10-year and 100-year events in b, and 1-year and 100-year events in c

on average during the 172 years, and the 10-year-return period and 100-year-return period increase by 8.06% and 12.00%, respectively. In addition, a decadal growth rate was calculated for each decade, for 0.56 and 0.47%/decade and the maximum decadal growth rate is 100 years, 0.70%/decade.

In the significance test, the hypothesis H0 is that the growth rate of the three extreme rainfall is 0. Otherwise, H1 is the growth rate of the three extreme rainfall is not 0, which means a significant increase. The $\alpha = 0.05$ was chosen as type I error, and as shown in the table 3.3 the p-value was less than 0.05, so H0 was rejected and H1 was accepted. The Spearman's rank test for the growth rates of the three extreme rainfalls showed a good agreement between all three extreme rainfalls, with a positive correlation of about 0.8, as figure 3.4.

The increase of rainfall in all three return periods is obvious, which means that the future will face more severe rainfall with increased daily rainfall intensity. There is a very large increase of extreme rainfall in the 100-year-return period.

This result also confirms what many previous studies have predicted. In using CMIP6 to predict future changes in extreme rainfall, Gründemann et al. concluded that daily land-based extreme rainfall could increase by 10.5% to 28.2% by the end of the century for the annual event and by 13.5% to 38.3% for the 100-year event, in both the low-emissions scenario and the high-emissions scenarios (Gründemann et al., 2022).

Global carbon dioxide emissions increased after the 19th century and climate warming has become an established fact. As of today, the temperature on Earth has increased by 1.1°C compared to the end of the 19th century, and what climatologists generally believe is that the temperature increase should be limited to 1.5°C by the end of this century for the sake of human development.

According to our calculations, the extreme rainfall increases by 9.73% in the 1-year return period, 8.06% in the 10-year return period and 12.00% in the 100-year return period for a 1.1°C temperature increase. This result has some reference value for the prediction of extreme rainfall in the future. For example, even if the temperature increase is controlled at 1.5°C,

extreme rainfall will still face an increasing trend, and if the high emission scenario continues, the intensity of extreme rainfall will be more significant at the global scale.

3.2. Extreme rainfall tendency in modern period (since 1950)

The climate warming associated with human forcing fits well with the observed warming, suggesting that about 104% of the total has come from human activity since the beginning of the ”modern” period in 1950 (Hausfather, 2017). In order to obtain the tendency of extreme rainfall changes since the modern era, data from the 1950 to the recent period were chosen for the analysis.

Table 3.4: The percentage of stations showing an increasing trend and the average growth rate since 1950

	1-year return period	10-year return period	100-year return period
The percentage of stations with an increase [%]	59.26	55.56	55.56
Average growth rate in all station since 1950 [%]	6.05	4.39	2.42
Average growth rate per decade since 1950 [%/decade]	0.84	0.61	0.34

There is an overall increasing trend of extreme rainfall since 1950, with nearly 56% of the stations with extreme rainfall changes greater than zero for the three return periods. Although only nearly 40 years of data were available, the extreme rainfall in the 1-year and 10-year return periods still showed a 4-6% growth rate, and the average growth in the 100-year return period was 2.42%, as shown in table 3.4.

All stations showed obvious changes, except for a few stations that showed little or no growth and decrease. And we can see that both positive and negative growth rates are evident in figure 3.5. Palermo, Italy had the largest extreme rainfall reduction rate, for the three return periods the rainfall intensity was reduced by more than 50%. But Padova, also an Italian city, had a large positive growth rate.

A t-test of the extreme rainfall intensity growth rate was considered to be a significant increase within the accepted range of α = 0.05, as shown in table 3.5. Similarly, the growth rates of the three extreme rainfall events were tested for Spearman’s rank in figure 3.7 and were found to exhibit the same good agreement between the different frequencies of extreme rainfall. However, the correlation between 1-year and 100-year extreme rainfall is weaker, at 0.65.

For the figure3.6, with the increase of the return period, the variance becomes larger and the interval of the distribution becomes wider. From the box plots, the extreme rainfall variability of the 100-year return period is the strongest because the distribution of the box part Q1-Q3 is the widest and the extreme values (including the maximum and minimum values) are more significant.

The calculated growth rate per decade showed that the annual and decadal extreme rainfall increase was greater than the previous case, data from 1850, 0.84 and 0.61 %/decade, respectively. However the centennial extreme rainfall growth rate was smaller, 0.34 %/decade, a result that is different from what we expected. We would have expected the 100-year return period to exhibit a much larger growth rate of rainfall with a large uncertainty. One possible explanation for this is that the 100-year extreme rainfall is large in both growth rate and decrease rate, and the display in the boxplot is a larger box range, thus averaging out the growth rate. The results show that although there is indeed a large uncertainty, the concentration of the growth rate distribution is small.

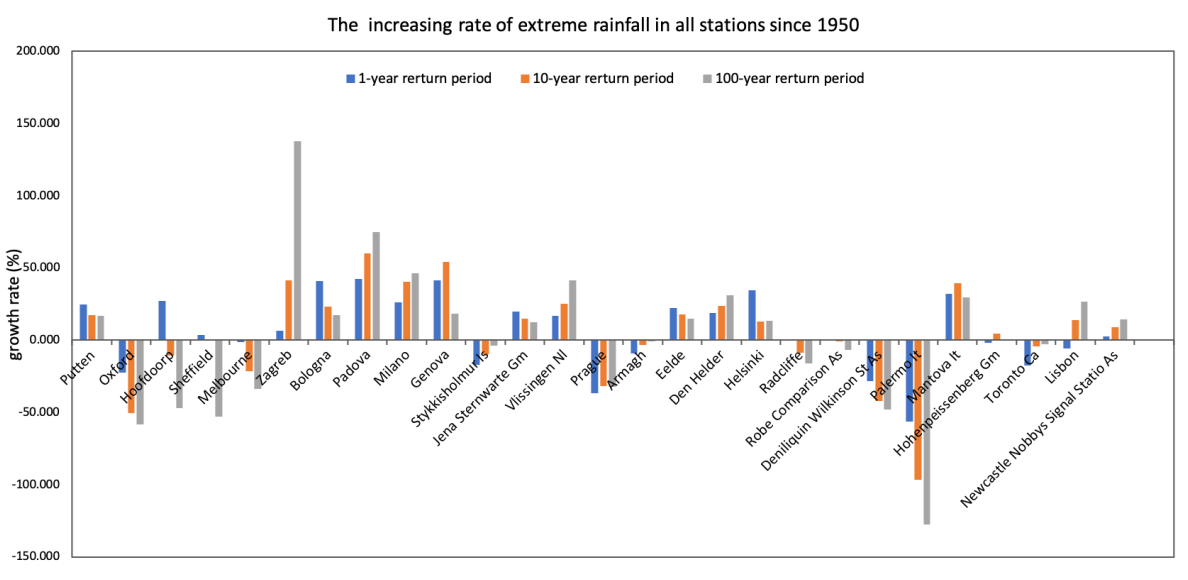

Figure 3.5: The increasing rate of extreme rainfall in all stations since 1950, [%]

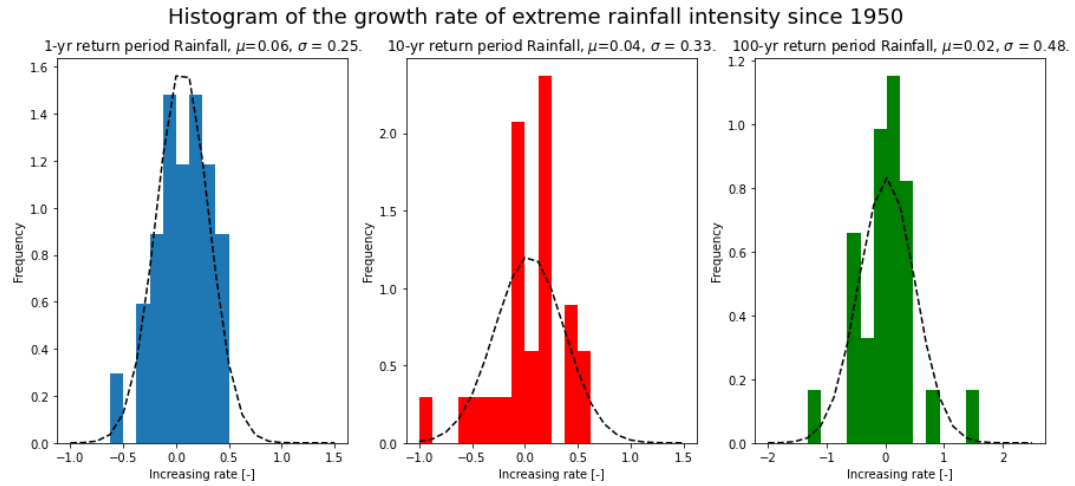

(a)

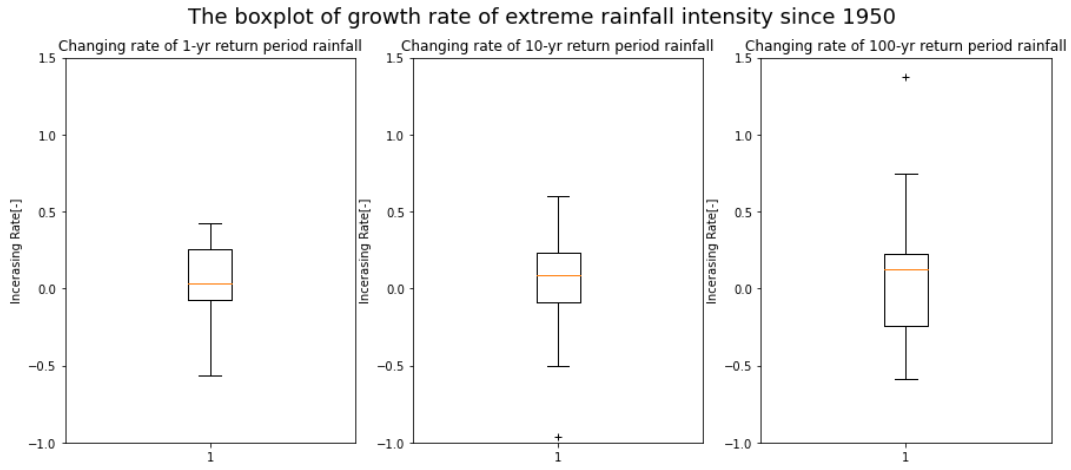

(b)

Figure 3.6: a.Histogram and b.boxplot of growth rate in all stations since 1950 for left.1-year-return period, middle.10-year-return period, right.100-year-rerturn period

Table 3.5: T-stastic test values and p-value of three extreme rainfall growth rate of data from 1950

	1-year return period	10-year return period	100-year return period
t-statistic	6.46	3.52	1.34
p-value	3.84E-7	7.98E-04	9.63E-02

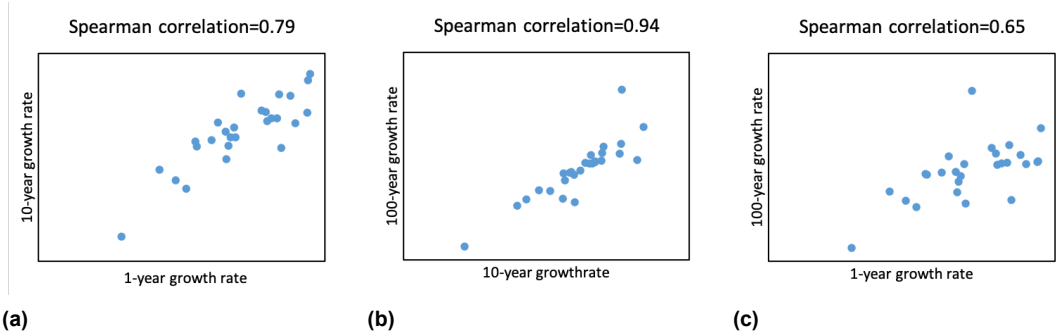

Figure 3.7: Spearman rank test of growthrate between three extreme rainfall since 1950, for 1-year and 10-year events in a, 10-year and 100-year events in b, and 1-year and 100-year events in c

3.3. Comparison and discussion

The global temperature has increased by 0.82 degrees Celsius when compared to the 1950 average (Roston, 2021). This is a very large increase compared to the 1.1 degrees Celsius from 1850-1900 to the present. Our expected result is that the intensity of extreme rainfall should increase rapidly after entering the modern period, and the longer the return period the more the rainfall should increase. However, this speculation is inaccurate because rainfall is influenced by very complex factors, not only temperature-related, but also by monsoons, The Southern Oscillation and land use, etc (Chang et al., 2012).

One very interesting note in the results is that since 1950, the rate of increase in extreme rainfall intensity, although also positive, has not increased as significantly as data since 1850. Looking at the decadal growth rate per decade for both time periods, it can be seen that the annual and decadal extreme rainfall grows faster after modern times, and the centennial growth becomes smaller after modern times, but still grows.

As can be seen in figure 3.5, a station that affects the rate of extreme rainfall growth obviously is Palermo, Italy, a station where the negative trend in the intensity of the three extreme rainfall types is very pronounced, with a 100-year-rate of rainfall reduction exceeding 100% and greatly pulling down the average growth rate. This trend coincides with Cislaghi et al.s' results, as figure 3.8, which showed a decrease in total and average annual rainfall in Palermo (southern Italy) from the mid 20th century to the beginning of the 21st century.

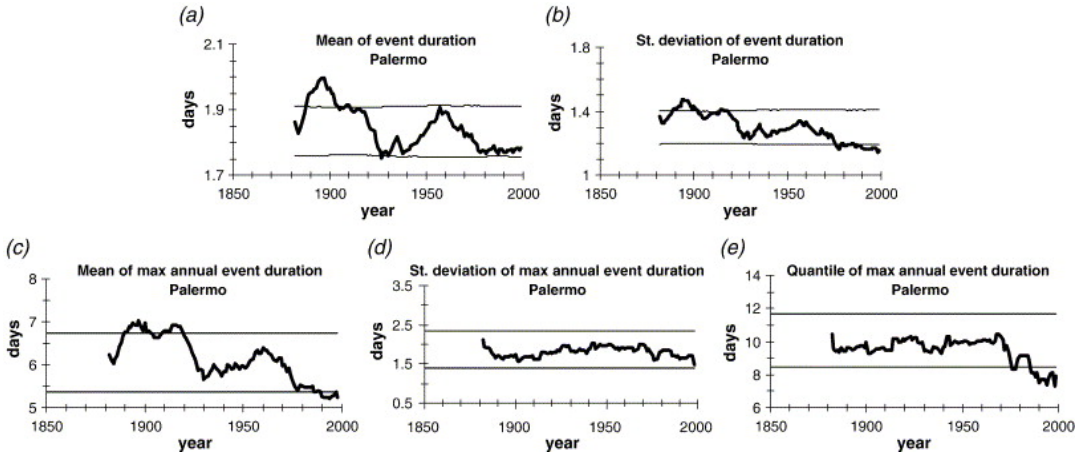

Figure 3.8: Rainy event duration in Palermo, (a) mean, (b) standard deviation, (c) mean of annual maximum, (d) standard deviation of annual maximum, (e) 30-year quantile of annual maximum (Cislaghi et al., 2005)

According to Gründemann et al., the growth rate of the rarest extreme rainfall should be the greatest. However, our results are contrary to this. One reason could be that rainfall growth rates were chosen for only 29 ultra-long stations, in which case very large increases or decreases would have a large impact on the overall results, such as Palermo. The effect of such extreme values would be reduced if data from more stations were selected. Another point is that the stations in this study are mainly in the European region, so it is a good reflection of the rainfall trend in Europe, while more research is needed for the analysis of rainfall in other continents.

In addition, the Spearman's rank test was also used for the detection of growth rates in two different time periods, as shown in Figure 3.9. It can be seen that the growth rates of the three types of extreme rainfall in the two time periods are hardly correlated, despite the fact that each showed an increasing trend, which also illustrates the volatility of extreme rainfall trends.

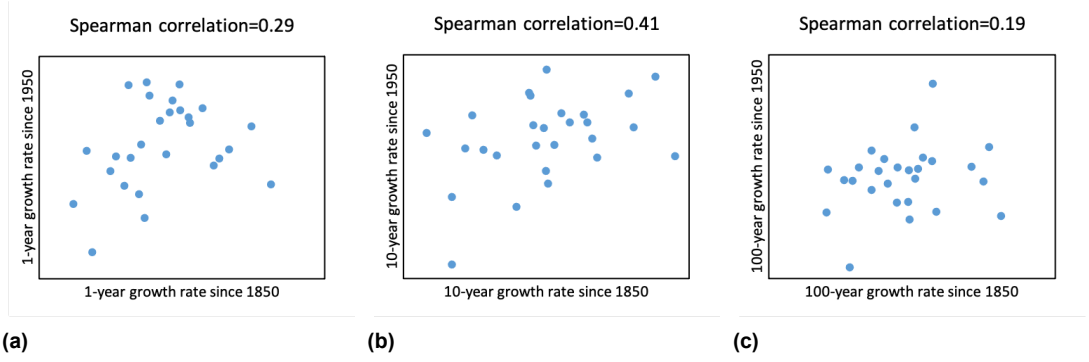

Figure 3.9: Spearman rank test of growthrate of extreme rainfall between data from 1850 and data from 1950, for 1-year events in a, 10-year events in b, and 100-year events in c

4

Conclusion

In this study, 29 stations with record years longer than 100 years and with fewer vacant records were selected, and the average data length was 174 years. The extreme rainfall for the 1-year, 10-year, and 100-year return periods were calculated using the MEV distribution in each 30 years and the following results were found.

1. Using all years of data, extreme rainfall was calculated and it was found that 70% of the stations showed an increasing trend in extreme rainfall intensity for all three return periods. The station with the most significant increase is Stykkisholmur, Iceland, where all three extreme rainfall periods show an increase of more than 100%.

2. For all data conditions, the extreme rainfall intensity increased by 9.73% on average for the 1-year return period, and 8.06% and 12.00% for the 10-year and 100-year return periods, respectively. 100-year return period had the most significant increase in extreme rainfall intensity, but also has the greatest variability.

3. Repeating the above process for years after the modern period in 1950, it is found that the extreme rainfall intensity at 56% of the stations shows an increasing trend during this period. At the same time, some sites, such as Palemo, show a very sharp decrease.

4. After 1950, the increasing trend of extreme rainfall is about 6% for the 1-year and 4% for 10-year return periods, and about 2.4% for the 100-year return period, which is different from the trend we guessed.

5. Comparing the growth rates per decade, it can be seen that rainfall in the 1-year and 10-year return periods grows faster in modern times, while the 100-year return period grows at a reduced rate in modern times.

5

Acknowledgement

The MEV package support for this study comes from Enrico Zorzetto. Metastatistical Extreme Value Analysis in Python (mevpy) is a function that provides MEV distribution and correlation methods developed for the analysis of MEV distribution of daily rainfall (Zorzetto, 2019).

For the different starting guess of x_0 attempts, I would like to thank Gründemann for helping me with the code.

References

Allen, M. R., & Ingram, W. J. (2002). Constraints on future changes in climate and the hydrologic cycle. *Nature*, *419*(6903), 224–232.

Elkhrachy, I. (2015). Flash flood hazard mapping using satellite images and gis tools: A case study of najran city, kingdom of saudi arabia (ksa). *The Egyptian Journal of Remote Sensing and Space Science*, *18*(2), 261–278.

Frame, D. J., Rosier, S. M., Noy, I., Harrington, L. J., Carey-Smith, T., Sparrow, S. N., Stone, D. A., & Dean, S. M. (2020). Climate change attribution and the economic costs of extreme weather events: A study on damages from extreme rainfall and drought. *Climatic Change*, *162*(2), 781–797.

Hallegatte, S., Green, C., Nicholls, R. J., & Corfee-Morlot, J. (2013). Future flood losses in major coastal cities. *Nature Climate Change*, *3*(9), 802–806.

EPA, U. (2021). Climate change indicators: U.s. and global precipitation.

Donat, M. G., Lowry, A. L., Alexander, L. V., O'Gorman, P. A., & Maher, N. (2016). More extreme precipitation in the world's dry and wet regions. *Nature Climate Change*, *6*(5), 508–513.

Trenberth, K. E., Dai, A., Rasmussen, R. M., & Parsons, D. B. (2003). The changing character of precipitation. *Bulletin of the American Meteorological Society*, *84*(9), 1205–1218.

O'Gorman, P. A., & Schneider, T. (2009). The physical basis for increases in precipitation extremes in simulations of 21st-century climate change. *Proceedings of the National Academy of Sciences*, *106*(35), 14773–14777.

Donat, M. G., Alexander, L. V., Yang, H., Durre, I., Vose, R., Dunn, R. J. H., Willett, K. M., Aguilar, E., Brunet, M., Caesar, J., Hewitson, B., Jack, C., Tank, A. M. G. K., Kruger, A. C., Marengo, J., Peterson, T. C., Renom, M., Rojas, C. O., Rusticucci, M., … Kitching, S. (2013). *118*(5), 2098–2118.

Held, I. M., & Soden, B. J. (2006). Robust responses of the hydrological cycle to global warming. *Journal of Climate*, *19*(21), 5686–5699.

Cislaghi, M., De Michele, C., Ghezzi, A., & Rosso, R. (2005). Statistical assessment of trends and oscillations in rainfall dynamics: Analysis of long daily italian series [Precipitation in Urban Areas]. *Atmospheric Research*, *77*(1), 188–202. https://doi.org/https://doi.org/10.1016/j.atmosres.2004.12.014

Partal, T., & Kahya, E. (2006). Trend analysis in turkish precipitation data. *Hydrological Processes*, *20*(9), 2011–2026. https://doi.org/10.1002/hyp.5993

Zhai, P., Zhang, X., Wan, H., & Pan, X. (2005). Trends in total precipitation and frequency of daily precipitation extremes over china. *Journal of Climate*, *18*(7), 1096–1108. https://doi.org/10.1175/JCLI-3318.1

Wang, Y., & Zhou, L. (2005). Observed trends in extreme precipitation events in china during 1961–2001 and the associated changes in large-scale circulation. *Geophysical Research Letters*, *32*(9).

Kunkel, K. E., Andsager, K., & Easterling, D. R. (1999). Long-term trends in extreme precipitation events over the conterminous united states and canada. *Journal of Climate*, *12*(8), 2515–2527. https://doi.org/10.1175/1520-0442(1999)012<2515:LTTIEP>2.0.CO;2

Zolina, O., Simmer, C., Belyaev, K., Kapala, A., & Gulev, S. (2009). Improving estimates of heavy and extreme precipitation using daily records from european rain gauges. *Journal of Hydrometeorology*, *10*(3), 701–716. https://doi.org/10.1175/2008JHM1055.1

Wang, H., & Xuan, Y. (2022). Spatial variation of catchment-oriented extreme rainfall in england and wales. *Atmospheric Research*, *266*, 105968.

Das, S., Kamruzzaman, M., & Islam, A. R. M. T. (2022). Assessment of characteristic changes of regional estimation of extreme rainfall under climate change: A case study in a tropical monsoon region with the climate projections from cmip6 model. *Journal of Hydrology*, *610*, 128002.

Yue, Z., Xiong, L., Zha, X., Liu, C., Chen, J., & Liu, D. (2022). Impact of thresholds on nonstationary frequency analyses of peak over threshold extreme rainfall series in pearl river basin, china. *Atmospheric Research*, *276*, 106269.

Fofana, M., Adounkpe, J., Larbi, I., Hounkpe, J., Djan'na Koubodana, H., Toure, A., Bokar, H., Dotse, S.-Q., & Limantol, A. M. (2022). Urban flash flood and extreme rainfall events trend analysis in bamako, mali. *Environmental Challenges*, *6*, 100449.

McBride, C. M., Kruger, A. C., & Dyson, L. (2022). Changes in extreme daily rainfall characteristics in south africa: 1921–2020. *Weather and Climate Extremes*, 100517.

Amponsah, W., Dallan, E., Nikolopoulos, E. I., & Marra, F. (2022). Climatic and altitudinal controls on rainfall extremes and their temporal changes in data-sparse tropical regions. *Journal of Hydrology*, *612*, 128090.

Marani, M., & Ignaccolo, M. (2015). A metastatistical approach to rainfall extremes. *Advances in Water Resources*, *79*, 121–126.

Marra, F., Nikolopoulos, E. I., Anagnostou, E. N., & Morin, E. (2018). Metastatistical extreme value analysis of hourly rainfall from short records: Estimation of high quantiles and impact of measurement errors. *Advances in Water Resources*, *117*, 27–39.

Miniussi, A., & Marani, M. (2020). Estimation of daily rainfall extremes through the metastatistical extreme value distribution: Uncertainty minimization and implications for trend detection. *Water Resources Research*, *56*(7).

Hosseini, S. R., Scaioni, M., & Marani, M. (2020). Extreme atlantic hurricane probability of occurrence through the metastatistical extreme value distribution. *Geophysical Research Letters*, *47*(1).

Min, S.-K., Zhang, X., Zwiers, F. W., & Hegerl, G. C. (2011). Human contribution to more-intense precipitation extremes. *Nature*, *470*(7334), 378–381.

Wang, L., Li, Y., Li, M., Li, L., Liu, F., Liu, D. L., & Pulatov, B. (2022). Projection of precipitation extremes in china's mainland based on the statistical downscaled data from 27 gcms in cmip6. *Atmospheric Research*, *280*, 106462.

Gründemann, G. J., van de Giesen, N., Brunner, L., & van der Ent, R. (2022). Rarest rainfall events will see the greatest relative increase in magnitude under future climate change. *Communications Earth & Environment*, *3*(1), 1–9.

Zorzetto, E., Botter, G., & Marani, M. (2016). On the emergence of rainfall extremes from ordinary events. *Geophysical Research Letters*, *43*(15), 8076–8082.

Gauthier, T. D. (2001). Detecting trends using spearman's rank correlation coefficient. *Environmental Forensics*, *2*(4), 359–362. https://doi.org/https://doi.org/10.1006/enfo.2001.0061

Wikipedia. (2022). Spearman's rank correlation coefficient. https://en.wikipedia.org/wiki/Spearman%27s_rank_correlation_coefficient

Myers, J. L., & Well, A. D. (2003). *Research design and statistical analysis*. Psychology Press. https://doi.org/10.4324/9781410607034

Hausfather, Z. (2017). Analysis: Why scientists think 100% of global warming is due to human. https://www.carbonbrief.org/analysis-why-scientists-think-100-of-global-warming-is-due-to-humans/

Roston, E. (2021). 2020 ties for hottest year in the hottest decade ever. https://www.bloomberg.com/news/articles/2021-01-14/global-warming-led-to-2020-tie-for-the-hottest-year-on-record?sref=fDPa8NQZ&leadSource=uverify%20wall

Chang, C.-P., Lei, Y., Sui, C.-H., Lin, X., & Ren, F. (2012). Tropical cyclone and extreme rainfall trends in east asian summer monsoon since mid-20th century. *Geophysical Research Letters*, *39*(18).

Zorzetto, E. (2019). Metastatistical extreme value analysis in python (mevpy). https://github.com/EnricoZorzetto/mevpy

A

Related tables and figures

Table A.1: Recording years of selected stations

Station name	Start year	End year	Length of recording years
Sydney Observatory Hill, As	1855	2022	167
Toronto,Ca	1840	2017	177
Armagh	1838	2008	170
Stykkisholmur	1856	2014	158
Helsinki	1845	2015	170
Radcliffe	1827	2014	187
Den Helder	1850	2022	172
Robe Comparison,As	1860	2022	162
Uppsala	1827	2022	195
Palermo,It	1797	2008	211
Prague	1804	2014	210
Eelde	1847	2022	175
Lisbon	1863	2013	150
Deniliquin Wilkinson St	1858	2014	156
Florence	1822	1979	157
Jena Sternwarte Gm	1826	2022	196
Mantova It	1840	2008	168
Vlissingen Nl	1854	2022	168
Newcastle Nobbys Signal Statio As	1862	2022	160
Hohenpeissenberg Gm	1781	2022	241
Hoofdoorp	1867	2014	147
Bologna	1813	2007	194
Oxford	1853	2008	155
Milano	1858	2006	148
Zagreb	1862	2004	142
Sheffield	1883	2008	125
Padova	1725	2013	288
Genova	1833	2008	175
Putten	1868	2014	146
Melbourne	1856	2013	157

Table A.2: Growth rates of extreme rainfall of all available data

Station	Growth rate(%)		
	1-year return period	10-year return period	100-year return period
Putten	12.872	15.712	8.762
Oxford	1.758	-0.471	15.895
Hoofdoorp	24.709	23.866	31.941
Sheffield	34.145	11.060	70.881
Melbourne	-1.353	8.420	8.091
Zagreb	2.446	3.323	29.912
Bologna	-2.185	-13.786	-14.599
Padova	4.384	8.652	18.615
Milano	16.484	33.378	63.546
Genova	16.279	41.390	53.031
Stykkisholmur Is	49.238	47.318	60.268
Jena Sternwarte Gm	9.323	4.742	-2.669
Vlissingen Nl	42.371	13.173	-7.029
Prague	3.831	9.066	14.890
Armagh	-8.532	-15.881	-23.335
Eelde	19.611	20.935	21.084
Den Helder	20.148	19.836	24.035
Helsinki	5.442	7.781	15.518
Radcliffe	-6.643	-6.231	-6.961
Robe Comparison As	11.597	5.539	2.904
Deniliquin Wilkinson St As	-21.927	-19.862	-34.196
Palermo It	-15.065	-19.800	-19.917
Mantova It	13.846	3.931	0.750
Hohenpeissenberg Gm	30.712	22.379	19.217
Toronto Ca	-3.620	-10.278	-18.232
Lisbon	28.658	34.834	29.224
Florence	1.201	4.273	7.746
Newcastle Nobbys Signal Statio As	-17.190	-27.487	-33.164

Table A.3: Growth rates of extreme rainfall of data since 1950

Station	Growth rate(%)		
	1-year return period	10-year return period	100-year return period
Putten	24.875	17.571	16.785
Oxford	-22.644	-50.467	-58.410
Hoofdoorp	27.278	-10.663	-46.806
Sheffield	3.361	-0.334	-53.124
Melbourne	-1.407	-21.374	-33.568
Zagreb	6.389	41.222	137.805
Bologna	40.959	23.141	17.433
Padova	42.513	60.217	74.731
Milano	26.229	40.667	46.491
Genova	41.258	54.416	18.178
Stykkisholmur Is	-16.910	-9.707	-3.739
Jena Sternwarte Gm	19.927	15.113	12.400
Vlissingen Nl	16.965	24.978	41.487
Prague	-36.692	-31.650	-32.467
Armagh	-9.230	-3.080	-0.982
Eelde	22.058	17.837	15.089
Den Helder	19.017	23.718	31.104
Helsinki	34.768	13.121	13.263
Radcliffe	-0.585	-8.882	-16.036
Robe Comparison As	0.680	-0.801	-6.607
Deniliquin Wilkinson St As	-28.165	-42.285	-48.054
Palermo It	-56.406	-96.655	-127.780
Mantova It	31.918	39.420	29.702
Hohenpeissenberg Gm	-2.053	4.577	0.461
Toronto Ca	-17.650	-4.436	-2.739
Lisbon	-5.772	13.969	26.561
Newcastle Nobbys Signal Statio As	2.563	9.005	14.186

Table A.4: Slopes of extreme rainfall of data since 1950

Station	Slope(mm/year)		
	1-year rerturn period	10-year rerturn period	100-year rerturn period
Putten	0.008	0.008	0.010
Oxford	-0.008	-0.028	-0.046
Hoofdoorp	0.009	-0.005	-0.035
Sheffield	0.001	0.000	-0.054
Melbourne	-0.001	-0.017	-0.040
Zagreb	0.003	0.026	0.108
Bologna	0.020	0.019	0.020
Padova	0.023	0.050	0.086
Milano	0.016	0.039	0.062
Genova	0.041	0.100	0.055
Stykkisholmur Is	-0.049	-0.045	-0.023
Jena Sternwarte Gm	0.056	0.072	0.085
Vlissingen Nl	0.051	0.113	0.251
Prague	-0.116	-0.178	-0.283
Armagh	-0.027	-0.013	-0.005
Eelde	0.063	0.078	0.089
Den Helder	0.057	0.110	0.194
Helsinki	0.097	0.061	0.088
Radcliffe	-0.002	-0.042	-0.104
Robe Comparison As	0.002	-0.004	-0.053
Deniliquin Wilkinson St As	-0.102	-0.324	-0.600
Palermo It	-0.249	-0.835	-1.780
Mantova It	0.153	0.317	0.350
Hohenpeissenberg Gm	-0.011	0.038	0.005
Toronto Ca	-0.087	-0.035	-0.030
Lisbon	-0.033	0.133	0.361
Newcastle Nobbys Signal Statio As	0.020	0.132	0.329